Surface Plasmons

DOI: 10.1002/anie.201002172

Fluorescence Studies into the Effect of Plasmonic Interactions on Protein Function**

*Jana B. Nieder, Robert Bittl, and Marc Brecht**

Plasmonic metal-nanostructures are an emerging tool for manipulating optical properties of fluorophores.[1–3] They are used for enhancing the sensitivity of fluorescence-based assays in drug discovery and high-throughput screenings as well as in immunoassays.[4] Even plasmon-assisted detection of biological reactions in vivo has been suggested.[5] The fast evolving range of applications for plasmonic nanomaterials make a deeper understanding of nanostructure–protein interactions necessary.

Interactions of plasmonic nanostructures with single fluorophores[6–8] and two-chromophore Förster resonance energy transfer (FRET) coupled systems[9] have been extensively studied, and first studies on biologically relevant systems with single chromophores[10] or with two coupled chromophores were published recently.[11] Studies of plasmonic interaction effects on more complex systems, with multiple chromophores coupled within one molecular assembly, are lacking.

Herein, we use a key protein of the photosynthetic apparatus, photosystem I (PSI), as a model for multichromophore FRET-coupled systems. The main function of PSI is to capture and convert solar energy into electrical energy. Around 100 chlorophyll molecules per monomer are involved in efficient light-harvesting and excitation energy transfer leading to light-induced charge separation in the reaction center (Figure 1).[12]

At low temperatures, specific chlorophyll molecules act as traps of the excitation energy, partially releasing their excitation energy as fluorescence (Figure 1c).[20–22] Single-molecule techniques make these different 'red chlorophyll' contributions discernible.[23] Their fluorescence can be used to analyze the excitation energy transfer[24] and in particular the influence of plasmonic interactions on the optical properties of PSI.

The samples used herein are PSI in buffer solution (PSI), PSI with colloidal gold nanoparticles of approximately 100 nm diameter (PSI-AuNP), and PSI on a heterogeneous

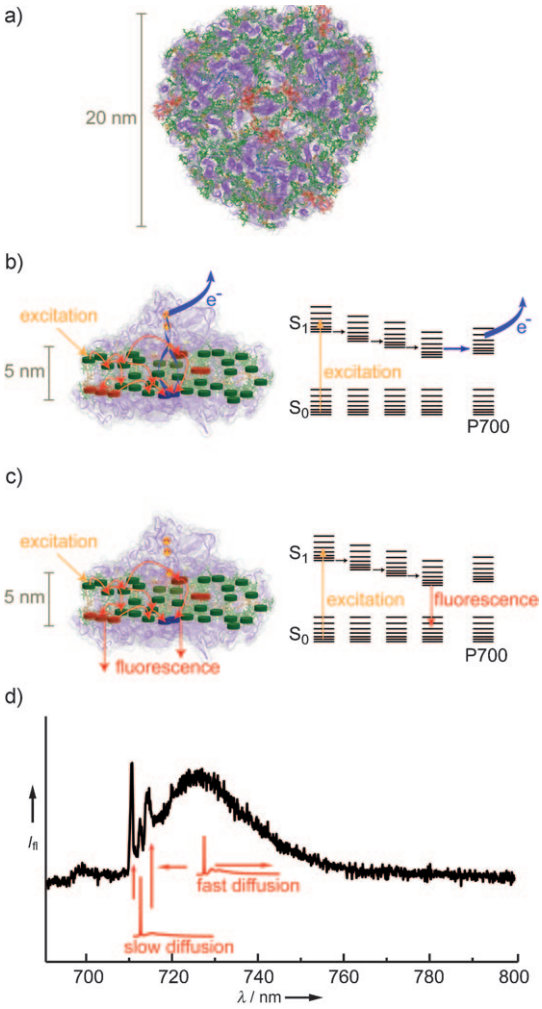

Figure 1. Photosystem I from oxygenic photosynthesis. a) Top view of trimeric PSI from cyanobacteria (protein data bank (PDB) entry: 1JB0).[12] In each monomer about 100 chlorophyll molecules (green) absorb excitation energy and transfer it to a chlorophyll dimer (blue) in the reaction center[13,14] which absorb at 700 nm (P700). The protein backbone is shown in violet. b) Illustration of excitation-energy transfer pathways at ambient temperatures overlaid on a side view of PSI (same coloring as in (a)) and an energy-level scheme. Upon excitation of P700 a charge-separated state across the membrane is formed.[13] Interestingly, also the red chlorophyll states (red) with lower excitation energies than P700 are involved in energy transfer. c) The transfer towards P700 is partially blocked and the red chlorophyll states become strongly fluorescent at low temperatures. d) A typical PSI fluorescence emission spectrum from an individual PSI complex. The spectra are composed of contributions from different red chlorophyll emitters. Their line widths differ, mainly due to unequal spectral diffusion.[15,16] The theoretical line shapes of single emitters that are not affected by spectral diffusion are given in red. These shapes were simulated by using the expressions and parameters in Refs. [17–19].

[*] J. B. Nieder, Prof. Dr. R. Bittl, Dr. M. Brecht
Fachbereich Physik, Freie Universität Berlin
Arnimallee 14, 14195 Berlin (Germany)
Fax: (+49) 308-385-6046
E-mail: marc.brecht@fu-berlin.de

[**] We thank Eberhard Schlodder (Technische Universität Berlin) for the PSI samples and helpful discussion and Prof. Stefanie Reich and Pascal Blümmel (Freie Universität Berlin) for the AFM characterization of the SIF. In addition, we acknowledge support from the Cluster of Excellence "Unifying Concepts in Catalysis" funded by the Deutsche Forschungsgemeinschaft.

Supporting information for this article is available on the WWW under http://dx.doi.org/10.1002/anie.201002172.

silver island film (PSI-SIF) (see Figure SI1 in the Supporting Information). For these three samples, fluorescence intensity scans, taken of the same sized area under identical experimental conditions, are shown in Figure 2a–c. An intensity

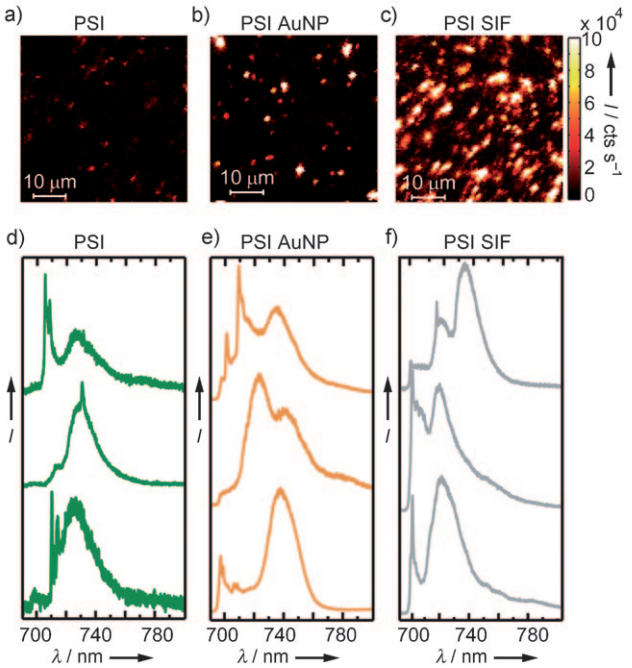

Figure 2. Fluorescence intensity scans of PSI (a), PSI-AuNP (b), and PSI-SIF (c) and three PSI spectra from different individual PSI complexes for each sample type (d–f). The fluorescence intensity scans were acquired with an integration time of 2 ms per pixel. An identical color scale ranging from 0 to 100 000 counts per second was chosen for comparison of the data. As a consequence the spot sizes increase in the scans of PSI-AuNP and PSI-SIF, where maximum intensities were about 50-times the threshold of 100 000 counts per second. The deviation of the spots from circular shapes can be attributed to the low imaging quality of the employed microscope objective at low temperatures. The spectra (d–f) were taken with an acquisition time of 40 s. For all experiments an excitation source with $\lambda_{exc} = 680$ nm and $P = 100$ µW was used.

increase from PSI to PSI-AuNP, and to PSI-SIF is clearly seen. Intensity scans of samples solely composed of AuNP or SIF without PSI also yield fluorescence signals (Supporting Information, Figure SI2), suggesting intrinsic signals from AuNP and SIF, and/or signals from impurities. Therefore, a determination of the fluorescence enhancement factors for the different plasmonic structures is not possible based on intensity information alone.

A spectral analysis of the intensity contributions present in the PSI-free samples of AuNP and of SIF shows that their signals are easily distinguishable from the PSI emission fingerprints and makes a separation of signals intrinsic to the nanostructure possible (Supporting Information, Figure SI3). In total 148 spectra were recorded for PSI in buffer, 158 for PSI-AuNP, and 72 for PSI-SIF.

In Figure 2d–f, representative PSI spectra for each of the sample types, measured under identical experimental conditions, are shown. The spectra are composed of characteristic contributions, appearing at different wavelength positions in the emission spectrum of PSI. The increased signal-to-noise ratios in the spectra from PSI-AuNP and PSI-SIF samples reflect enhanced fluorescence emission. The line widths of the different red chlorophyll contributions within the spectra of individual PSI remain largely preserved (Figure 2); unexpectedly, the increased exciton flux migrating through PSI upon coupling to a plasmonic nanostructure does not significantly increase the probability for fluctuations that would result in line broadening.

The integrated fluorescence intensities of all the individual PSI complexes are given as histograms in Figure 3. The intensity histogram (green) of uncoupled PSI has a nearly

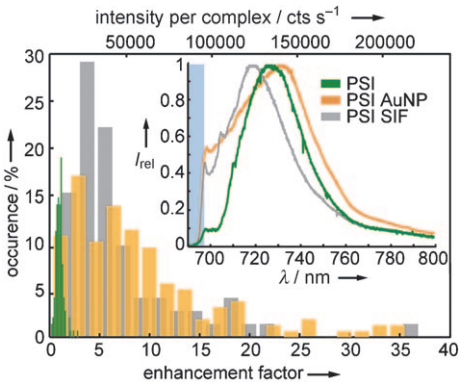

Figure 3. Intensity histograms of signals from PSI (green), PSI-AuNP (orange), and PSI-SIF (gray). The intensities for the individual complexes were obtained from spectrally resolved data. The counts detected in the wavelength interval from 690 nm to 800 nm were integrated after subtraction of a constant background to eliminate dark counts and stray light. The intensity ranges for the different samples were each divided into 20 bins. Inset: mean spectra of 142 individual PSI spectra from PSI, 158 spectra from PSI-AuNP, and 72 spectra from PSI-SIF. The wavelength range suppressed by the cut-off filter is marked in blue.

Gaussian shape, while the histograms for PSI-AuNP and PSI-SIF steeply increase to a maximum value and decay approximately exponentially to higher intensities. Enhancement factors (Figure 3, bottom x-axis) give the relative intensity of individual PSI-AuNP and PSI-SIF with respect to the mean intensity of uncoupled PSI. Maximum observed enhancements are 36 for PSI-SIF and 37 for PSI-AuNP and the average enhancements are 7 and 9, respectively. This significant metal-enhanced fluorescence (MEF) of PSI coupled to AuNP or SIF is of the same order of magnitude as that reported for other fluorophore–metal-nanostructure interactions.[11,25–29]

The inset in Figure 3 shows the normalized average spectra of all the PSI, PSI-AuNP, and PSI-SIF complexes, respectively. The AuNPs lead to an increased line width of the PSI fluorescence (Γ_{FWHM}(PSI) = 33 nm versus Γ_{FWHM}(PSI-AuNP) = 52 nm; FWHM = full width at half maximum); in contrast, the line width of SIF-coupled PSI remains virtually unchanged (Γ_{FWHM}(PSI-SIF) = 37 nm). The peak position of fluorescence emission for PSI-SIF is blue-shifted by 8 nm to 719 nm compared with uncoupled PSI (727 nm), whereas the

peak position of the PSI-AuNP (732 nm) is red-shifted relative to uncoupled PSI. Both plasmonic structures lead to strongly increased fluorescence at the short-wavelength side of the fluorescence emission indicating strongly enhanced fluorescence deactivation of the higher energy antenna pigments, which show virtually no fluorescence emission in the absence of plasmonic structures. Relative fluorescence intensities between 698–705 nm and the respective fluorescence maximum intensity increase from around 10% for PSI to 40–60% and 50–60% for PSI-SIF and PSI-AuNP, respectively. The average enhancement factors in this wavelength range are as large as 40–60 for both structures and the enhancement reaches maximal values of about 200 for PSI-SIF and about 400 for PSI-AuNP. Thus, the shape of the average spectra of PSI-AuNP and PSI-SIF shows considerable deviations from the average spectrum of uncoupled PSI. This situation is in contrast to single chromophore systems and two-chromophore FRET-coupled systems interacting with similar plasmonic structures, where nearly uniform fluorescence enhancement was observed.[11,30,31] Only minor spectral shifts were observed for albumin in gold-nanoparticle biconjugates, which were explained by conformational changes of the water-soluble protein on the metal surface.[32] The rather uniform fluorescence enhancement of organic chromophores is because the plasmon spectra of the nanostructures used are rather featureless[33,34] over the fluorescence emission profiles of the chromophores studied. The fluorescence emission of PSI at low temperatures is of comparable width to the systems studied at room temperature to date,[11,30,31] and larger structural changes are unlikely, since PSI complexes retain their charge-separation capability even in close proximity to nanostructures or metal surfaces.[35–39] Thus, for PSI a rather uniform fluorescence enhancement could be expected. The observed non-uniform enhancement can be understood taking into account the properties of multichromophore assemblies.

The FRET efficiency between chromophores depends on their spectral overlap, separation, and orientation.[40] The specific coupling conditions between the chromophores lead to a characteristic set of transition rates (Figure 4a). In PSI this is optimized for the efficient excitation of the reaction center.

The interaction between pigments and plasmonic structures is also strongly distance- and orientation-dependent.[40] A distance-dependent enhancement curve calculated for a fluorophore coupled to a AuNP of 100 nm diameter shows quenching at distances shorter than approximately 2 nm, maximum enhancement at approximately 13 nm, and an exponential decay to longer distances indicating an absence of interactions at around 80 nm.[6] In contrast to other studies, where PSI was prepared in defined orientation on metal surfaces and metal nanoparticles,[35–37] in our case, PSI is randomly oriented towards the plasmonic structures. This feature is a possible origin of the observed broad distribution of enhancement factors.

The size of a PSI trimer, in which around 300 chlorophyll pigments confined in an approximately cylindrical structure measuring around 20 nm in diameter and approximately 5 nm in height, makes coupling scenarios possible where some

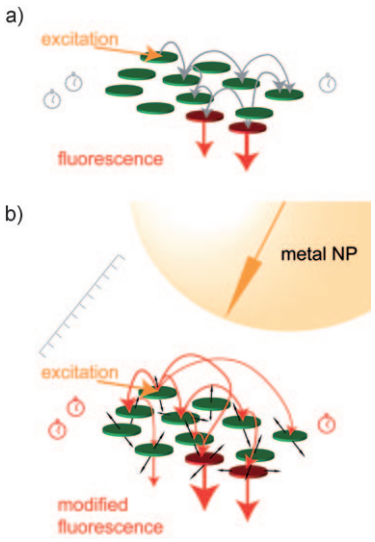

Figure 4. Visualization of excitation energy transfer pathways in a multichromophore FRET-coupled system. a) Without plasmonic interaction: Specific coupling conditions between the chromophores lead to a characteristic set of transition rates indicated by gray arrows. Clocks indicate the respective excited state lifetimes. b) With plasmonic interaction: The set of transition rates is modified through to plasmonic coupling, which is distance- and orientation-dependent indicated by the ruler and black arrows, respectively. Additional excitation energy transfer pathways (red) illustrate the origin of the modified system response.

chlorophyll molecules are quenched and others are subjected to maximum fluorescence enhancement. As fluorescence enhancement is correlated with a decrease in the fluorescence lifetime,[34] the balance between fluorescence and other deactivation channels, such as energy transfer, can be changed. Plasmonic interaction alters Förster interaction distances between chromophores.[9] In one donor–acceptor pair the Förster radius increases from 8.3 to 13 nm as a result of plasmonic interaction.[9] This effect can change the exciton distribution within PSI by involving additional chromophores in excitation energy transfer (Figure 4b).

In conclusion, our experiments show an altered fluorescence of PSI upon interaction with AuNP and SIF. Particularly the higher energy chlorophyll molecules with site-energies close to that of the reaction center show increased deactivation through fluorescence emission, thereby reducing the efficiency of energy transfer towards the site of charge separation (P700), and thus altering the protein function. We suppose that altered responses can generally be expected for multichromophore FRET-coupled systems near plasmonic nanostructures. These findings have to be considered when aiming at nanostructure-assisted bio-applications.

Experimental Section

For the single-molecule experiments, PSI from *Thermosynechococcus elongatus* were diluted to a concentration of 3 pM in a Tricin buffer solution containing 0.02% w/v *n*-dodecyl-β,D-maloside (β-DM) as a detergent preventing PSI aggregation.[16] Less than 1 μL of this solution was placed between two cover slips. To couple PSI to gold

nanoparticles (PSI-AuNP) an excess of colloidal gold nanospheres of approximately 100 nm diameter[41] was added to the PSI buffer solution (AuNP:PSI ratio ca.12:1). The preparation of the SIF was performed as described in Chowdhury et al.[42] AFM characterization shows size distributions ranging from 200–400 nm in width and 20–550 nm in height (Supporting Information, Figure SI1). The PSI-SIF sample was prepared by placing the diluted PSI sample between an untreated and the SIF-coated coverslip, which was placed on the back side of the sample with respect to the incident beam. For the single-molecule fluorescence measurements a home-built low-temperature confocal spectrometer,[16] with a $\lambda_{exc} = 680$ nm diode laser attenuated to 100 μW as excitation source and an Avalanche Photodiode (Perkin–Elmer) or a LN_2-cooled CCD camera (Princeton Instruments) as detector was used. The temperature for all experiments was $T = 1.4$ K.

Received: April 13, 2010
Revised: August 30, 2010
Published online: November 29, 2010

Keywords: nanostructures · photosynthesis · proteins · single-molecule studies · surface plasmon resonance

[1] J. R. Lakowicz, *Plasmonics* **2006**, *1*, 5 – 33.
[2] E. Fort, S. Gresillon, *J. Phys. D* **2008**, *41*, 013001.
[3] M. Steiner, C. Debus, A. V. Failla, A. J. Meixner, *J. Phys. Chem. C* **2008**, *112*, 3103 – 3108.
[4] K. Aslan, I. Gryczynski, J. Malicka, E. Matveeva, J. R. Lakowicz, C. D. Geddes, *Curr. Opin. Biotechnol.* **2005**, *16*, 55 – 62.
[5] Y.-E. Koo Lee, R. Smith, R. Kopelman, *Annu. Rev. Anal. Chem.* **2009**, *2*, 57 – 76.
[6] P. Anger, P. Bharadwaj, L. Novotny, *Phys. Rev. Lett.* **2006**, *96*, 113002.
[7] J. R. Lakowicz, K. Ray, M. Chowdhury, H. Szmacinski, Y. Fu, J. Zhang, K. Nowaczyk, *Analyst* **2008**, *133*, 1308 – 1346.
[8] Y. Fu, J. R. Lakowicz, *Laser Photonics Rev.* **2009**, *3*, 221 – 232.
[9] J. Zhang, Y. Fu, M. H. Chowdhury, J. R. Lakowicz, *J. Phys. Chem. C* **2007**, *111*, 11784 – 11792.
[10] Y. Fu, J. Zhang, J. R. Lakowicz, *Biochem. Biophys. Res. Commun.* **2008**, *376*, 712 – 717.
[11] S. Mackowski, S. Wörmke, A. J. Maier, T. H. P. Brotosudarmo, H. Harutyunyan, A. Hartschuh, A. O. Govorov, H. Scheer, C. Bräuchle, *Nano Lett.* **2008**, *8*, 558 – 564.
[12] P. Fromme, P. Jordan, N. Krauss, *Biochim. Biophys. Acta Bioenerg.* **2001**, *1507*, 5 – 31.
[13] B. Gobets, R. van Grondelle, *Biochim. Biophys. Acta Bioenerg.* **2001**, *1507*, 80 – 99.
[14] N. V. Karapetyan, E. Schlodder, R. van Grondelle, J. P. Dekker in *Advances in Photosynthesis and Respiration*, *Vol. 24* (Eds.: J. H. Golbeck), Springer, Dordrecht, **2007**, pp. 177 – 192.
[15] M. Brecht, *Mol. Phys.* **2009**, *107*, 1955 – 1974.
[16] M. Brecht, H. Studier, A. F. Elli, F. Jelezko, R. Bittl, *Biochemistry* **2007**, *46*, 799 – 806.
[17] J. Pieper, J. Voigt, G. Renger, G. J. Small, *Chem. Phys. Lett.* **1999**, *310*, 296 – 302.
[18] V. Zazubovich, S. Matsuzaki, T. W. Johnson, J. M. Hayes, P. R. Chitnis, G. J. Small, *Chem. Phys.* **2002**, *275*, 47 – 59.
[19] M. Rätsep, T. W. Johnson, P. R. Chitnis, G. J. Small, *J. Phys. Chem. B* **2000**, *104*, 836 – 847.
[20] M. Byrdin, I. Rimke, E. Schlodder, D. Stehlik, T. A. Roelofs, *Biophys. J.* **2000**, *79*, 992 – 1007.
[21] L. O. Palsson, C. Flemming, B. Gobets, R. van Grondelle, J. P. Dekker, E. Schlodder, *Biophys. J.* **1998**, *74*, 2611 – 2622.
[22] A. N. Melkozernov, *Photosynth. Res.* **2001**, *70*, 129 – 153.
[23] F. Jelezko, C. Tietz, U. Gerken, J. Wrachtrup, R. Bittl, *J. Phys. Chem. B* **2000**, *104*, 8093 – 8096.
[24] M. Brecht, V. Radics, J. B. Nieder, R. Bittl, *Proc. Natl. Acad. Sci. USA* **2009**, *106*, 11857 – 11861.
[25] Y. Chen, K. Munechika, D. S. Ginger, *Nano Lett.* **2007**, *7*, 690 – 696.
[26] S. Kühn, U. Hakanson, L. Rogobete, V. Sandoghdar, *Phys. Rev. Lett.* **2006**, *97*, 017402.
[27] P. P. Pompa, L. Martiradonna, A. Della Torre, F. Della Sala, L. Manna, M. De Vittorio, F. Calabi, R. Cingolani, R. Rinaldi, *Nat. Nanotechnol.* **2006**, *1*, 126 – 130.
[28] S. Vukovic, S. Corni, B. Mennucci, *J. Phys. Chem. C* **2009**, *113*, 121 – 133.
[29] J. Enderlein, *Biophys. J.* **2000**, *78*, 2151 – 2158.
[30] E. Matveeva, Z. Gryczynski, J. Malicka, I. Gryczynski J. R. Lakowicz, *Anal. Biochem.* **2004**, *334*, 303 – 311.
[31] K. Ray, R. Badugu, J. R. Lakowicz, *J. Am. Chem. Soc.* **2006**, *128*, 8998 – 8999.
[32] L. Shang, Y. Z. Wang, J. G. Jiang, S. J. Dong, *Langmuir* **2007**, *23*, 2714 – 2721.
[33] J. R. Lakowicz, C. D. Geddes, I. Gryczynski, J. Malicka, Z. Gryczynski, K. Aslan, J. Lukomska, E. Matveeva, J. Zhang, R. Badugu, J. Huang, *J. Fluoresc.* **2004**, *14*, 425 – 441.
[34] J. R. Lakowicz, Y. B. Shen, S. D'Auria, J. Malicka, J. Y. Fang, Z. Gryczynski, I. Gryczynski, *Anal. Biochem.* **2002**, *301*, 261 – 277.
[35] H. Krassen, A. Schwarze, B. Friedrich, K. Ataka, O. Lenz, J. Heberle, *ACS Nano* **2009**, *3*, 4055 – 4061.
[36] R. A. Grimme, C. E. Lubner, D. A. Bryant, J. H. Golbeck, *J. Am. Chem. Soc.* **2008**, *130*, 6308 – 6311.
[37] L. Frolov, O. Wilner, C. Carmeli, I. Carmeli, *Adv. Mater.* **2008**, *20*, 263 – 266.
[38] N. Terasaki et al., *Angew. Chem.* **2009**, *121*, 1613 – 1615; *Angew. Chem. Int. Ed.* **2009**, *48*, 1585 – 1587 (see Supporting Information for full author list).
[39] A. O. Govorov, I. Carmeli, *Nano Lett.* **2007**, *7*, 620 – 625.
[40] K. Aslan, S. N. Malyn, C. D. Geddes, *Chem. Phys. Lett.* **2008**, *453*, 222 – 228.
[41] BBInternational, Product Ananlysis: mean diameter: 97.1 nm; coefficient of variation < 8% Technical Report, **2008**.
[42] M. H. Chowdhury, K. Ray, K. Aslan, J. R. Lakowicz, C. D. Geddes, *J. Phys. Chem. C* **2007**, *111*, 18856 – 18863.

